Spatio-temporal couplings for controlling group velocity in longitudinally pumped seeded soft X-ray lasers

Adeline Kabacinski, Eduardo Oliva, Fabien Tissandier, Julien Gautier, Michaela Kozlová, Jean-Philippe Goddet, Igor Andriyash, Cédric Thaury, Philippe Zeitoun, Stéphane Sebban

2. Supplementary Information:

Item	**Present?**	**Filename** **Whole original file name including extension. i.e.: Smith_SI.pdf. The extension must be .pdf**	**A brief, numerical description of file contents.** **i.e.: *Supplementary Figures 1-4, Supplementary Discussion, and Supplementary Tables 1-4.***
Supplementary Information	Yes	Supplementary_information_NPHOT_2022_07_00928A.pdf	Supplementary discussion : - Dephasing length and need for plasma dispersion compensation in the case of seeded SXRLs (figure 1 and 2, + 1 reference) - Energy measurements and definition of energy extraction (figure 3)
Reporting Summary	No		

Spatio-temporal couplings for controlling group velocity in longitudinally pumped seeded soft X-ray lasers

Adeline Kabacinski[1], Eduardo Oliva[2], Fabien Tissandier[1], Julien Gautier[1], Michaela Kozlová[3,4], Jean-Philippe Goddet[1], Igor Andriyash[1], Cédric Thaury[1], Philippe Zeitoun[1], Stéphane Sebban[1,*]

[1]Laboratoire d'Optique Appliquée, ENSTA-Paristech, CNRS, Ecole Polytechnique, Institut Polytechnique de Paris, 828 Bv des Maréchaux, 91762 Palaiseau, France
[2]Instituto de Fusión Nuclear "Guillermo Velarde" and Departamento de Ingeniería Energética, E.T.S.I. Industriales, Universidad Politécnica de Madrid, Spain
[3]ELI Beamlines Project, Institute of Physics CAS, Praha 8, Czech Republic
[4]Institute of Plasma Physics CAS, Praha 8, Czech Republic
[*]stephane.sebban@ensta-paris.fr

Abstract : Controlling the group velocity of an ultrashort laser pulse by spatio-temporal couplings has been proposed to overcome inherent limitations in laser-plasma interactions. We here report how this method improves the performance of a seeded soft X-ray laser (SXRL), which intrinsically suffers from the group velocity mismatch between the infrared pump beam, used to generate the plasma amplifier, and the soft X-ray seed beam. The energy extraction was measured to be 3 times higher when the pump group velocity varies from 0.55c to 1.05c. Moreover we demonstrate that the SXRL pulse duration is governed by the pump beam velocity. By compensating the natural group velocity mismatch, the SXRL pulse duration can be kept constant along its propagation, resulting in energetic pulses (up to 2 µJ) as short as 350 fs. Such achievements constitute the first experimental demonstration of the so-called "flying focus effect" to an application by controlling the group velocity of a high intensity laser pulse propagating in a plasma.

Laser-plasma interaction arouses great interest as it abounds in applications in scientific, medical and industrial domains[1,2]. However, a plasma is a negative dispersion medium in which the propagation velocity of a wave depends on its wavelength: the longer the wavelength, the slower the wave propagates. This effect becomes more and more significant as the plasma density increases, and often has limiting consequences. For instance, in laser-wakefield accelerators[3], dephasing originates from the difference between the laser and the electron bunch velocities. This causes electrons to move into a phase region of the plasma that is decelerating, therefore restricting the acceleration length and the electron beam energy gain. In photon accelerators[4], high plasma densities are required as they produce a strong refractive index gradient and consequently a strong associated frequency shift. Nevertheless, these favorable conditions are accompanied by stronger plasma dispersion resulting in faster decoupling between the photon beam and the ionization wave, and thus in shorter interaction lengths. In longitudinally pumped seeded SXRLs, the plasma dispersion results in a desynchronization between the infrared beam used to pump the amplifier and the soft X-ray seed beam. It inevitably leads to a temporal stretching of the SXRL pulse and to a poor energy extraction from the energy contained in the ASE to the amplified seed. Moreover, high electron densities and long amplifiers are the key for SXRLs optimization, but in these conditions the natural desynchronization between the gain and the seed gets so strong that it prevents amplification (see Supplementary information Figure 1 and Figure 2). For further improvements of the source, compensating the plasma dispersion will therefore become the most limiting factor and will have to be systematically addressed.

A hope to overcome these bottlenecks is to control the group velocity of the laser beam along the Rayleigh length. Several techniques have been proposed for this purpose[5,6,7,8]. One of them is based on the use of two spatio-temporal couplings (STCs). Pulse Front Curvature (PFC, quantified by α [fs/cm²] equivalent in the far field to longitudinal chromatism) induces the

different spectral components of a beam to be focused at different longitudinal positions. Coupled with temporal chirp (quantified by β [fs²]) which changes the timing between these different wavelengths, PFC enables to control the velocity of the peak intensity of an ultrashort pulse on axis[9]. This phenomenon is known as the "flying focus effect". Depending on the amount of those STCs, the peak intensity can be deposited either from the back to the front of the focal region, or in the opposite direction. Subluminal to superluminal pulses have therefore been demonstrated[10] paving the way for novel control of laser-plasma interactions. With this method, the ability to adjust the velocity of a femtosecond pulse in vacuum has been demonstrated[11], as well as the ability to drive ionization waves of arbitrary velocity which has been experimentally observed with moderate laser intensities[12,13]. Although simulations promise breakthroughs for photon acceleration[14] or Raman amplification[15], direct experimental application with high intensity lasers has not been reported yet to date.

The present work applies this "flying focus effect" to a high intensity laser pulse (4 x 10^{18} W/cm²) propagating in a plasma and demonstrates the benefit of controlling group velocity in laser-plasma interaction in the benchmark case of a longitudinally pumped seeded SXRL. The development of SXRLs has been motivated by the hope to carry out, at laboratory scale, single-shot dynamical studies in the nanometric wavelength domain. Seeded SXRLs turn out to be energetic sources[16] available in a wide spectral range[17,18,19]. Their amplifying medium is a highly charged plasma, created by the interaction of an intense laser beam with a solid[20] or a gas[21]. The population inversion is achieved thanks to collisional excitation, resulting in a strong amplification of spontaneous emission (ASE) in the soft X-ray range (typically 3,5 µJ). The spatial properties of the SXRL beam can be improved by seeding the amplifier with high-order harmonics (HH)[22,23] resulting in a coherent gaussian-like diffraction-limited beam[24]. The harmonics and the seeded SXRL energies being respectively below 1 nJ and close to 2 µJ, the amplification factor is around 2000.

Nevertheless, seeding process has intrinsic limitations as the soft X-ray seed naturally propagates faster than the infrared pump into the plasma amplifier. This group velocity mismatch increases at high electron densities, which are required to generate short gain life time as well as intense amplification[25,26]. For instance, at an electron density $n_e = 10^{20}$ cm^{-3}, the soft X-ray beam basically propagates at c, whereas the infrared pump beam only propagates at 0.97c. It consequently conducts to a desynchronization between the arrival of the seed and the sub-ps gain window[25] preventing from centimeter scale amplification length. For transient SXRLs, the use a of a traveling wave has been proposed to match the heating of the plasma with the propagation of the soft X-rays photons in the plasma column[27]. However, this technique is not suitable for longitudinal geometry and has never been used to compensate the plasma dispersion.

In this work, we investigate how the desynchronization between the gain and the seed affects the energy and pulse duration of SXRL by harnessing spatio-temporal couplings (PFC and temporal chirp) to control the group velocity of the pump beam. The amount of PFC is varied by inserting chromatic doublets of infinite focal length in the pump beam, and the amount of temporal chirp is adjusted with the distance between the gratings of the pump compressor (see figure 1, see Methods). PFC enables to deposit the intensity of the pump beam in a line along the longitudinal direction. Temporal chirp changes the delay at which a given spectral component arrives at a given longitudinal position. The group velocity of the pump beam can therefore be set at a value different than the natural group velocity induced by plasma dispersion at a given electron density.

First, we investigated the amount of energy contained in the amplified seed, and its proportion with respect to the energy obtained in purely ASE regime (i.e. the maximum energy that can be extracted) while varying the synchronization between the seed and the gain. This measurement has been performed respectively in figure 2 (a) for α = 4 fs/cm², (b) for α = -2 fs/cm² and (c) for α = -9 fs/cm². The uncertainty on α was ± 1 fs/cm². The pump beam group

velocity was controlled, for a given α which should be different from 0 to permit the adjustment, with the amount of temporal chirp. The variation of the seeded soft X-ray laser signal versus β is shown in blue in figure 2. As |β| is increased, the SXRL signal naturally decreases due to the drop of the pump intensity induced by the pulse stretching[21]. Without group velocity adjustment, this decrease is supposed to be symmetrical with respect to the optimum chirp. However, an asymmetric behaviour is observed: in (a), the signal sharply drops for positive values of chirp and diminishes rather smoothly for negative chirps. In (c), this asymmetry is reversed with a sharp drop for negative chirps and a smoother decrease for positive chirps. In (b) the signal seems almost symmetrical, the coefficient α being close to 0.

On the same graph, the group velocity with respect to temporal chirp is plotted in red. The error band corresponds to an uncertainty of ± 1 fs/cm² on α and 500 fs² (corresponding to a systematic error of 100 µm on the optimum compression) on β. The shape of the group velocity with respect to β depends on α. In particular, the group velocity displays an asymptote at chirp $\beta = \frac{2f^2\alpha}{\omega_0}$ (see Methods). The location of this asymptote therefore depends on α and explains well the asymmetric behaviour observed on the seeded signal. Indeed, the desynchronization between the seed and the gain region gets stronger and faster as the mismatch between the soft X-rays and the infrared is increased. When the infrared propagates at c, the seed stays synchronized with the gain optimum along the propagation. For small mismatches, the seed is desynchronized with the gain optimum but keeps being amplified in different gain regions. When the mismatch increases, the seed meets weaker gain regions during shorter times and is therefore less and less amplified. The side of the asymptote in the group velocity is a critical region where the signal drops sharply due to a significant desynchronization. On the contrary, the signal declines more smoothly when the group velocity gently goes away from c.

The energy extraction is also shown (in green) in figure 2. It is calculated as the ratio of the energy contained in the amplified seed to the energy measured in the ASE (without seeding, see Methods and Supplementary information Figure 3). In (a) the energy extraction increases from 19 ± 6\% to 59 ± 4\% between 0.55c and 1.05c obtained respectively for around -30000 fs² and a suited chirp of 2000 fs². We measure an optimum energy extraction of 58 ± 16\% in (b) and 37 ± 6\% in (c), obtained for the investigated group velocities which are the closest to c in each case. The energy extraction is therefore optimal when compensating the natural dispersion of the plasma, the seed being synchronized with the optimum gain, and is degraded when the group velocity mismatch increases. It can be noted that the experimental conditions were stable during a given scan at fixed α. However, due to difficulties to maintain identical experimental conditions on a day-to-day basis (laser energy and beams overlapping), the optimum energy extraction was not constant for the investigated configurations. We emphasize that the dispersion compensation does not necessarily need a huge sacrifice in pump intensity : for instance in (a), the group velocity is equal to c for β = 300 fs² which corresponds to a pulse duration of 37 fs (instead of 30 fs at optimum chirp). It results in an intensity of 3 x 10^{18} W/cm² (instead of 4 x 10^{18} W/cm²), sufficient to generate the lasing ions.

In a second time, we studied how the SXRL pulse duration depends on the infrared pump beam group velocity. Pulse duration measurements have been performed at an electron density close to n_e = 7 x 10^{19} cm^{-3}, using a recently developed technique[26]. Figure 3 shows with blue symbols the measured SXRL RMS pulse duration with respect to the gas jet length for different group velocities. Linear regressions of the pulse duration measurements with respect to the jet length are plotted in red. The graph shows different behaviours depending on the group velocity mismatch. For a strong desynchronization (in (a), v_g = 1.09c ± 0.04c), the pulse duration increases quickly with respect to the jet length with a slope of (89 ± 10) fs/mm. For a minor desynchronization (in (c), v_g = 0.98c ± 0.02c), pulse duration increases more gently. Measurements have been performed for two different electron densities for this group velocity (n_e = 6 x 10^{19} cm^{-3} and n_e = 8 x 10^{19} cm^{-3}). The difference in their respective slopes can be explained by the uncertainty on the group velocity, here comprised between 0.96c and

c for both cases but not necessarily identical. In the case (b) where v_g = 1.00c ± 0.03c, the pulse duration remains nearly constant with respect to the jet length, with a slope of (6 ± 10) fs/mm. Experimentally, the stronger the group velocity mismatch, the more the SXRL pulse is stretched when propagating along the amplifier.

This behaviour has been investigated using the DAGON 3D Maxwell-Bloch code[28] for an electron density $n_e = 8 \times 10^{19}$ cm^{-3}. The simulated amplified pulse intensity (false color) and population inversion (grayscale) for different group velocities and after different propagation lengths are shown in figure 4. When the group velocity is equal to c (upper row), the SXRL pulse duration remains constant along the propagation in the plasma as the seed beam is synchronized with the gain region. On the contrary, when the group velocity is different from c (lower row, here 0.95c), the soft X-rays propagate faster than the infrared. This desynchronization results in a stretching of the SXRL during its propagation as the tail of the soft X-ray pulse is progressively amplified.

In figure 5 (a), the RMS simulated pulse duration is plotted with respect to the jet length and for a group velocity ranging from 0.95c to 1.1c. The SXRL pulse duration is almost constant to around 350 fs at c, is increasing from 350 fs to 900 fs between 1 and 10 mm at 1.05c, and from 350 fs to 1.7 ps between 1 and 10 mm at 1.1c. Therefore, at a given electron density and a given plasma amplifier length, the pulse duration can be adjusted in a wide range thanks to the control of the group velocity by STCs. The simulated RMS pulse duration with respect to group velocity after 10 mm of propagation is shown in figure 5 (b). The pulse duration is clearly reduced (from 1.7 ps at 1.1c to 350 fs at c) when locking the pump and seed velocities. It can be noted that the simulated pulse duration is here 20 fs shorter at 0.99c than at c. This can probably be explained by the RMS criterion as it takes into account the shape of the pulse which depends on the group velocity.

Consequent increase of the SXRL seed amplification can be achieved resorting to high electron densities and long amplifying media[25,26] crucially requiring plasma dispersion compensation (see Supplementary information Figure 2). Moreover, as demonstrated here, the energy which can be gained by lengthening the amplifier is obtained at the expense of the pulse duration if the dispersion is not compensated. This cost gets increasingly important when the electron density and the amplifier length are raised as the desynchronization gets stronger. For a natural group velocity v_g = 0.97c at an electron density close to 10^{20} cm^{-3}, simulations predict a stretching from 350 fs at 1 mm up to 640 fs at 10 mm, i.e. a pulse almost twice longer than it would be if the pump velocity was artificially set at c thus allowing to keep the pulse duration constant along the propagation. Furthermore, as established previously, controlling the pump group velocity also allows for an optimization of the energy extraction. Therefore, dispersion compensation offers great potential for SXRLs optimization and fosters opportunities for applications requiring high intensities.

Controlling the natural velocity mismatch between the pump and the seed beams also paves the way for applications requiring pulses at the femtosecond time scale. Collisional SXRL pulse duration has been ranging for decades between 1.1 ps[29] and 100 ps[16]. It has been experimentally shown only recently that femtosecond durations are achievable by quenching the amplification while raising the electron density of the plasma amplifier[26]. Figure 3 (c) illustrates that the pulse length can be significantly shortened by combining the pulse duration reduction induced by the increase of electron density (here from 6 to 8 x 10^{19} cm^{-3}) and by the control of the pump group velocity (here set at 0.98c ± 0.02c). It ensues a measured RMS duration of 350 ± 200 fs in agreement with the simulations, obtained with energetic pulses (up to 2 µJ) generated with a 10 mm plasma amplifier, which is the shortest collisional SXRL pulse duration ever reported.

In summary, the suppression of the group velocity mismatch improves the performance of current state-of-the-art SXRLs, and offers a considerable potential to continue on this path.

The compensation of natural dispersion in SXRLs fosters opportunities for many applications requiring ultrashort pulses, or high intensities such as non linear XUV optics[30], and provides an avenue to perform single-shot high resolution dynamical studies at the femtosecond time scale[31] with a table-top source. This study also represents the first direct application of the "flying focus effect" to a high intensity laser pulse propagating in a plasma, and illustrates that fundamental limitations of laser-plasma interactions induced by plasma dispersion can be overcome thanks to STCs, opening prospects in a wide scope of domains such as photon acceleration or laser wakefield acceleration.

Acknowledgements : This work is supported by ”Investissement d’Avenir” (ANR-10-LABX-0039-PALM (F.T. and S.S.) and ANR-18-EURE-0014 (A.K.)) and has received funding from the European Union’s Horizon 2020 research and innovation program under grant agreement No. 654148 Laserlab-Europe. This work is also supported by Grant agency of the Czech Republic, project number 18-27340S (M.Z.). The authors acknowledge support from COST (European Cooperation in Science and Technology) for funding the Action TUMIEE (CA17126) supporting this work. This work is also supported by the Universidad Politécnica de Madrid and the Comunidad Autónoma de Madrid, línea de actuación estímulo a la investigación de jóvenes doctores, project CROM and the Spanish Ministerio de Ciencia e Innovación through a Ramón y Cajal RYC2018-026238-I fellowship (E.O.), and by Plan Estatal de Investigación Científica, Técnica y de Innovación (Spain Ministerio de Ciencia e Innovación), grant PID2021-124129OB-I00 (E.O.).

Author Contributions Statement : A.K., F.T., J.G, M.K. and S.S. designed and built the experiment, and performed the measurements. A.K. analysed the experimental results. E.O. developed the DAGON code. E.O. and A.K. performed the numerical simulations. J.-P.G. operated the upgraded laser system of ‘Salle Jaune’. I.A., C.T. and P.Z. supported the project. All the authors contributed to the writing of the paper.

Competing Interests Statement : The authors declare no competing interests.

Tables (empty)

Figure Legends :

Figure 1 (SXRL&vg.ppt) : **Experimental setup**. Generation of the seeded soft X-ray laser with a longitudinal pumping scheme. The group velocity v_g^{pump} of the pump beam is controlled thanks to the adjustment of spatio-temporal couplings. Pulse Front Curvature, characterized by the parameter α, is varied by inserting chromatic doublets of infinite focal length in the beam before compression. Temporal chirp, characterized by β, is adjusted by varying the distance between the gratings of the compressor.

Figure 2 (Extraction.ppt) : **Measurements of the impact of the group velocity on the SXRL energy.** In blue, seeded SXRL signal with respect to temporal chirp β. In green, energy extraction as a ratio of energy contained in the seeded beam to the energy in ASE. Measurement points in blue and green are presented as mean values (N = 5) +/- SEM. In red, group velocity of the infrared with respect to temporal chirp. The measurements are performed for three different values of α : respectively +4 fs/cm² in (a), -2 fs/cm² in (b), and -9 fs/cm² in (c).

Figure 3 (Measurements.ppt) : **Measurements of the impact of the group velocity on the SXRL pulse duration.** Evolution of the pulse duration with respect to the jet length for different group velocities. In blue, measurements of the RMS pulse duration of the SXRL with respect to the jet length. Measurements have been performed for different group velocities of the pump beam (respectively larger, equal and smaller than c) at an electron density close to $n_e = 7 \times 10^{19}$ cm^{-3}. In red, linear regressions of these measurements. Small symbols are used for

individual points, large symbols are used for averaging over few shots (N = 5). Data are presented as mean values +/- SEM.

Figure 4 (Simulations3D.ppt) : **3D simulations of the amplified SXRL pulse.** Simulated amplified pulse intensity (false color) and population inversion (grayscale) for a group velocity of c (upper row), and 0.95c (lower row) after respectively 1 mm, 5 mm and 10 mm from left to right.

Figure 5 (Simulations.ppt) : **Simulations of the impact of the group velocity on the SXRL pulse duration.** Simulations of the RMS SXRL pulse duration at $n_e = 8 \times 10^{19}$ cm^{-3} (a) with respect to the jet length for different group velocities of the infrared, (b) with respect to the infrared group velocity for a 10 mm long jet.

References :

1. Eliezer, S. & Mima, K. Applications of Laser–Plasma Interactions (Series in Plasma Physics, 2009).
2. Malka, V. et al. Principles and applications of compact laser–plasma accelerators. Nat. Phys. 4, 447–453, DOI: https://doi.org/10.1038/nphys966 (2008).
3. Esarey, E., Schroeder, C. B. & Leemans, W. P. Physics of laser-driven plasma-based electron accelerators. Rev. Mod. Phys. 81, 1229-1285, DOI : https://doi.org/10.1103/RevModPhys.81.1229 (2009).
4. Mendonca, J. T. Theory of Photon Acceleration (Series in Plasma Physics, 2000).
5. Andriyash, I., Balcou, P. & Tikhonchuk, V. Collective properties of a relativistic electron beam injected into a high intensity optical lattice. The Eur. Phys. J. D 65, 533–540, DOI: https://doi.org/10.1140/epjd/e2011-20254-5 (2011).
6. Debus, A. et al. Circumventing the dephasing and depletion limits of laser-wakefield acceleration. Phys. Rev. X 9, DOI: https://doi.org/10.1103/PhysRevX.9.031044 (2019).
7. Palastro, J. P. et al. Dephasingless laser wakefield acceleration. Phys. Rev. Lett. 124, DOI: https://doi.org/10.1103/PhysRevLett.124.134802 (2020).
8. Caizergues, C., Smartsev, S., Malka, V. & Thaury, C. Phase-locked laser-wakefield electron acceleration. Nat. Photonics 14, 475–479, DOI: https://doi.org/10.1038/s41566-020-0657-2 (2020).
9. Sainte-Marie, A., Gobert, O. & Quéré, F. Controlling the velocity of ultrashort light pulses in vacuum through spatio-temporal couplings. Optica 4, 1298–1304, DOI: https://doi.org/10.1364/OPTICA.4.001298 (2017).
10. Froula, D. H. et al. Spatiotemporal control of laser intensity. Nat. Photonics 12, 262–265, DOI: https://doi.org/10.1038/s41566-018-0121-8 (2018)
11. Jolly, S. W., Gobert, O., Jeandet, A. & Quéré, F. Controlling the velocity of a femtosecond laser pulse using refractive lenses. Opt. Express 18, 4888–4897, DOI: https://doi.org/10.1364/OE.384512 (2020).
12. Turnbull, D. et al. Ionization waves of arbitrary velocity. Phys. Rev. Lett. 120, 225001, DOI: https://doi.org/10.1103/PhysRevLett.120.225001 (2018).
13. Franke, P. et al. Measurement and control of large diameter ionization waves of arbitrary velocity. Opt. Express 27, DOI: https://doi.org/10.1364/OE.27.031978 (2019).
14. Howard, A. J. et al. Photon acceleration in a flying focus. Phys. Rev. Lett. 123, 124801, DOI: https://doi.org/10.1103/PhysRevLett.123.124801 (2018).
15. Turnbull, D. et al. Raman amplification with a flying focus. Phys. Rev. Lett. 120, 024801, DOI: https://doi.org/10.1103/PhysRevLett.120.024801 (2018).
16. Rus, B. et al. Multimillijoule, highly coherent x-ray laser at 21 nm operating in deep saturation through double-pass amplification. Phys. Rev. A 66, 063806, DOI: https://doi.org/10.1103/PhysRevA.66.063806 (2002).
17. Rockwood, A. et al. Compact gain-saturated x-ray lasers down to 6.85 nm and amplification down to 5.85 nm. Optica 5, DOI: https://doi.org/10.1364/OPTICA.5.000257 (2018).
18. Lemoff, B. E., Barty, C. P. & Harris, S. E. Femtosecond-pulse-driven, electron-excited xuv lasers in eight-times-ionized noble gases. Opt. Lett. 19, 569–571, DOI: https://doi.org/10.1364/OL.19.000569 (1994).
19. Tissandier, F. et al. Two-color soft x-ray lasing in a high-density nickel-like krypton plasma. Phys. Rev. Lett. 124, DOI: https://doi.org/10.1103/PhysRevLett.124.133902 (2020).
20. Wang, Y. et al. High-brightness injection-seeded soft-x-ray-laser amplifier using a solid target. Phys. Rev. Lett. 97, DOI: 10.1103/PhysRevLett.97.123901 (2006).
21. Sebban, S. et al. Demonstration of a ni-like kr optical-field-ionization collisional soft x-ray laser at 32.8 nm. Phys. Rev. Lett. 89, DOI: https://doi.org/10.1103/PhysRevLett.89.253901 (2002).
22. Zeitoun, P. et al. A high-intensity highly coherent soft x-ray femtosecond laser seeded by a high harmonic beam. Nature 431, 426–429, DOI: https://doi.org/10.1038/nature02883 (2004).
23. Wang, Y. et al. Phase-coherent, injection-seeded, table-top soft-x-ray lasers at 18.9 nm and 13.9 nm. Nat. Photonics 2, 94–98, DOI: https://doi.org/10.1038/nphoton.2007.280 (2008).
24. Goddet, J. P. et al. Aberration-free laser beam in the soft x-ray range. Opt. Lett. 34, 2438–2440 (2009).
25. Depresseux, A. et al. Table-top femtosecond soft x-ray laser by collisional ionization gating. Nat. Photonics 9, 817–821,DOI: https://doi.org/10.1038/nphoton.2015.225 (2015).
26. Kabacinski, A. et al. Femtosecond soft x-ray lasing in dense collisionaly-pumped plasma. Phys. Rev. Res. 4, L032009,DOI: https://doi.org/10.1103/PhysRevResearch.4.L032009 (2022).
27. Klisnick, A. et al. Transient pumping of a ni-like ag x-ray laser with a subpicosecond pump pulse in a traveling-wave irradiation geometry. J. Opt. Soc. Am. B 17, 1093–1097, DOI: 10.1364/JOSAB.17.001093 (2000).
28. Oliva, E. et al. Dagon: a 3d maxwell-bloch code. In Proc. SPIE 10243, X-ray Lasers and Coherent X-ray Sources: Development and Applications, vol. 10243, DOI: https://doi.org/10.1117/12.2265044 (2017).

29. Wang, Y. et al. Measurement of 1-ps soft x-ray laesr pulses from an injection-seeded plasma amplifier. Phys. Rev. A 79,023810, DOI: https://doi.org/10.1103/PhysRevA.79.023810 (2009).
30. Helk, T. et al. Table-top extreme ultraviolet second harmonic generation. Sci. Adv. 7, DOI: 10.1126/sciadv.abe2265 (2021).
31. Sokolowski-Tinten, K. et al. Femtosecond x-ray measurement of coherent lattice vibrations near the lindemann stability limit. Nature 422, 287–289, DOI: https://doi.org/10.1038/nature01490 (2003).

Methods :

Laser system

The experiment was conducted at the Laboratoire d'Optique Appliquée with the 'Salle Jaune' Ti:Sa laser system, which delivers 3 beams at 1 Hz around a central wavelength of 820 nm: a pump beam (1.5 J, 30 fs), a waveguiding beam composed of two pulses -an "ignitor" pulse (150 mJ, 30 fs) followed 900 ps later by a "heater" pulse (700 mJ, 600 ps)-, a HH driver beam (30 mJ, 30 fs). A part of the pump beam (20 mJ, 30 fs) is used for pulse duration measurements.

SXRL

The soft X-ray amplifier at 32.8 nm was generated by focusing the intense infrared pump beam with a spherical mirror (f' = 700 mm) into the krypton gas jet, resulting in an intensity of 4 x 10^{18} W/cm² enabling the generation of the lasing ion. A population inversion is then achieved thanks to an efficient pumping by hot electrons, allowing for a lasing of the $3d^9 4d_{J=0} \rightarrow 3d^9 4p_{J=1}$ transition of nickel-like krypton at 32.8 nm[21]. The gas jet length can be adjusted under vacuum between 4.5 and 10 mm thanks to a motorized blade covering a part of the slit nozzle.

To overcome the strong refraction of the pump beam induced by the plasma, an optically preformed plasma waveguide was implemented using the second beam composed of two pulses ("ignitor"+"heater"), which is focused by an axicon lens over the whole gas length[32]. The electron density builds up as electrons generated by the "ignitor" get heated and foster avalanche collisional ionization. The natural hydrodynamic plasma expansion then starts and the generated electrons are ejected out of the optical axis, therefore allowing pump beam propagation[33]. The waveguide transmission was assessed around 40\% by integrating the whole energy of the beam profile imaged at the entrance and at the output of the plasma channel. The electron density of the plasma amplifier was measured with a Mach-Zender interferometer.

The soft X-ray seed[22,23] is implemented by focusing an infrared driver beam into a gas cell filled with argon. The on-target intensity was assessed at about 2 x 10^{14} W/cm². The 25th harmonic signal was optimized by changing the gas pressure and the beam energy, tuning the beam aperture with a motorized iris, adjusting the longitudinal position of the lens, and spectrally tuned onto the amplifier ASE laser line at 32.8 nm by chirping the HH driver beam. The seeding was fulfilled by imaging the harmonic output at the entrance of the plasma amplifier, using a 5° grazing-incidence gold-coated toroidal mirror in a 1.5–1 m conjugation. Special attention has been paid to spatial and temporal matching. The spatial coupling of the HH beam and the SXRL gain region was done in the infrared by overlapping the infrared driver with the focal spot of the pump. The temporal overlap between the HH signal and the SXRL amplification period was approached by synchronizing the infrared driver and the pump beams with an accuracy of 30 fs.

Adjustment of the pump beam group velocity

The group velocity of the pump beam was controlled by adjusting the amount of two spatio-temporal couplings: the Pulse Front Curvature (PFC) and the temporal chirp. PFC is equivalent to longitudinal chromatism in the far field, and is quantified by its strength α in fs/cm² given by:

$$z(\omega) = 2cf^2\alpha\frac{\Delta\omega}{\omega}$$

where z(ω) is the longitudinal position of the focusing plane of the frequency ω, f is the focal length (here f' = 700 mm for the spherical mirror focusing the pump beam), and Δω the frequency offset with respect to ω_0 the central frequency of the pump beam. To introduce in practice a precise amount of PFC in the beam, chromatic doublets of infinite focal length are inserted before compression[11]. Here the quantity of PFC has been varied working either with 2 doublets (α= +4 fs/cm²), either with a single doublet (α= -2 fs/cm²), either without doublet (α= -9 fs/cm²). The coefficient α was measured with an uncertainty of ± 1 fs/cm². It can be noted that the amount of PFC can also be adjusted dynamically by changing the longitudinal position of a single chromatic doublet inserted in a divergent beam[34].

The second STC needed is the temporal chirp, given by the parameter $\beta = -\left(\frac{d^2\varphi}{d^2\omega}\right)_{\omega_0}$, the second order derivative of the spectral phase in fs². In practice, the amount of temporal chirp of the pump beam was adjusted by changing the distance between the gratings of the compressor, since the coefficient β is proportionnal to it.

The group velocity v_g can finally be derived from the following formula :

$$\frac{v_g}{v_g^{nat}} = \frac{1}{1 - \left(\frac{\omega_0}{2f^2}\right)\left(\frac{\beta}{\alpha}\right)}$$

v_g^{nat} being the natural group velocity given by $v_g^{nat} = c\sqrt{1 - \frac{n_e}{n_c^{\lambda}}}$, with n_e the electron density of the plasma and n_c^{λ} the critical density at a given wavelength.

Energy measurements

The energy measurement was performed using a 25° off-axis soft X-ray parabola of focal length 200 mm, a deflecting plane mirror at a 80° incidence angle and a soft X-ray camera of resolution 1024 × 1024 pixels. The interferential multilayer coating of the parabola designed to yield a high reflectivity at 32.8 nm was deposited at the Institut d'Optique, France. The system images a plane at about 1.4 m from the soft X-ray plasma source with a magnification of 0.6. The signal has been measured in purely ASE regime (without seeding), and within the amplified seed (with seeding). The energy extraction has been derived as the ratio of the energy contained in the amplified seed to the total energy contained in the ASE, which represents the maximum energy that can be extracted (See supplementary information Figure 3 for more details). These measurements have been performed for three different α coefficients and for a distance between the compression gratings varied in the range -7 to +7 mm around the optimum compression. Error bars were determined by repeatibility over few shots (standard error of the mean).

Pulse duration measurements

The SXRL pulse duration was measured using a single-shot temporal profiler described in[26]. The measurement is based on a pump-probe technique allowing to measure the transient reflectivity of a laser-damaged soft X-ray mirror using the 32.8 nm laser as a probe. A soft X-ray multilayer is irradiated simultaneously with the SXRL beam and with an intense infrared femtosecond pulse in a travelling wave geometry. The envelope of the temporal profile can be retrieved with a resolution as short as 200 fs. Uncertainties have been determined taking into account this resolution and the repeatability over few shots. Measurements have been performed at electron densities close to 7 x 10^{19} cm^{-3}, for different jet lengths and group velocities of the pump beam.

3D Maxwell-Bloch simulations

Simulations have been performed using the DAGON 3D Maxwell-Bloch code[28,35]. The group velocity of the pump beam can be varied as an input parameter of this code, which models the full spatio-temporal structure of the amplification of high-order harmonics along the pulse propagation in a krypton plasma amplifier. The creation and evolution of the plasma waveguide is modelled with the 2D radiative hydrodynamics code ARWEN[36,37]. This code solves the equations of compressible fluid-dynamics coupled to energy transfer processes: electronic diffusion, radiative transfer and laser propagation and absorption. The resulting density profile is fed to a 2D axysymmetric Particle-In-Cell code, FBPIC[38]. This code solves Maxwell´s equations and the relativistic motion equations for the macroparticles that model the plasma. The temporal dynamics of the lasing ion and population inversion is modelled with the collisional-radiative code OFIKinRad[39]. Non-equilibrium effects are taken into account by solving a Fokker-Planck equation to compute the electron energy distribution function and, afterwards, the cross sections. The output of FBIC and OFIKinRad is used by DAGON to compute the temporal dynamics of the plasma amplifier. DAGON solves the set of 3D Maxwell-Bloch equations in the paraxial and slowly varying envelope approximation, taking into account the temporal dynamics of the amplifier medium. The three-dimensional aspect of the code is required to take into account the waveguide and the inhomogeneities of the plasma. These inhomogeneities mainly come from the overionization induced in regions where the intensity reaches the threshold to produce higher charged ions due to focusing effects[40]. In addition to this, the code also takes into account the 3D stochastic structure of the Amplified Spontaneous Emission. We modelled a 100 µm x 100 µm x 10 mm amplifier, using a mesh consisting in 100 x 100 x 2000 cells. The timestep was fixed to 10 fs.

Data availability : The main datasets supporting the findings of this study are provided within the paper. Additionnal data are available from the corresponding authors upon reasonable request.

Methods-only references :

32. Chou, M. C. et al. Dramatic enhancement of optical-field-ionization collisional-excitation x-ray lasing by an optically preformed plasma waveguide. Physcial Rev. Lett. 99, DOI: 10.1103/PhysRevLett.99.063904 (2007).
33. Oliva, E. et al. Hydrodynamic evolution of plasma waveguides for soft-x-ray amplifiers. Phys. Rev. E 97, DOI: https://doi.org/10.1103/PhysRevE.97.023203 (2018).
34. Kabacinski, A. et al. Measurement and control of main spatio-temporal couplings in a cpa laser chain. J. Opt. 23, 06LT01,DOI: 10.1088/2040-8986/abf88f (2021).
35. Oliva, E. et al. 3d multi-scale modelling of plasma-based seeded soft x-ray lasers. The Eur. Phys. J. D 75, DOI: https://doi.org/10.1140/epjd/s10053-021-00298-y (2021).
36. Ogando, F. & Velarde, P. Development of a radiation transport fluid dynamic code under amr scheme. J. Quant. Spectrosc.& Radiat. Transf. 71, 541, DOI: https://doi.org/10.1016/S0022-4073(01)00096-6 (2001).
37. Cotelo, M. et al. Simulation of radiative shock waves in xe of last pals experiments. High Energy Density Phys. 17, 68 –73, DOI: http://dx.doi.org/10.1016/j.hedp.2014.12.002 (2015). 10th International Conference on High Energy Density Laboratory Astrophysics.
38. Lehe, R., Kirchen, M., Andriyash, I. A., Godfrey, B. B. & Vay, J.-L. A spectral, quasi-cylindrical and dispersion-free particle-in-cell algorithm. Comput. Phys. Commun. 203, 66–82, DOI: https://doi.org/10.1016/j.cpc.2016.02.007 (2016).
39. Cros, B. et al. Characterization of the collisionally pumped optical-field-ionized soft-x-ray laser at 41.8nm driven in capillary tubes. Phys. Rev. A 73, 033801, DOI: https://doi.org/10.1103/PhysRevA.73.033801 (2006).
40. Tuitje, F. et al. Nonlinear ionization dynamics of hot dense plasma observed in a laser-plasma amplifier. Light. Sci. & Appl.9, DOI: https://doi.org/10.1038/s41377-020-00424-2 (2020).

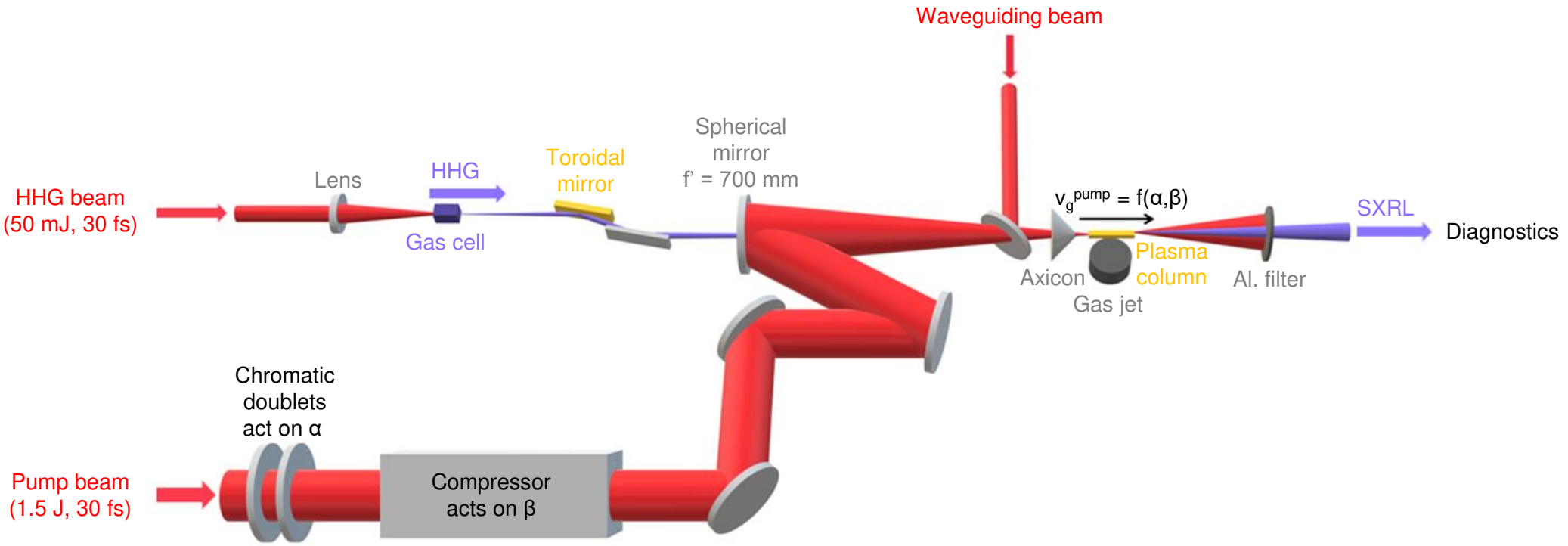
Waveguiding beam
HHG beam
(50 mJ, 30 fs)
Lens
HHG
Gas cell
Toroidal
mirror
Spherical
mirror
f' = 700 mm
$v_g^{pump} = f(\alpha,\beta)$
SXRL
Diagnostics
Axicon
Plasma
column
Gas jet
Al. filter
Chromatic
doublets
act on α
Pump beam
(1.5 J, 30 fs)
Compressor
acts on β

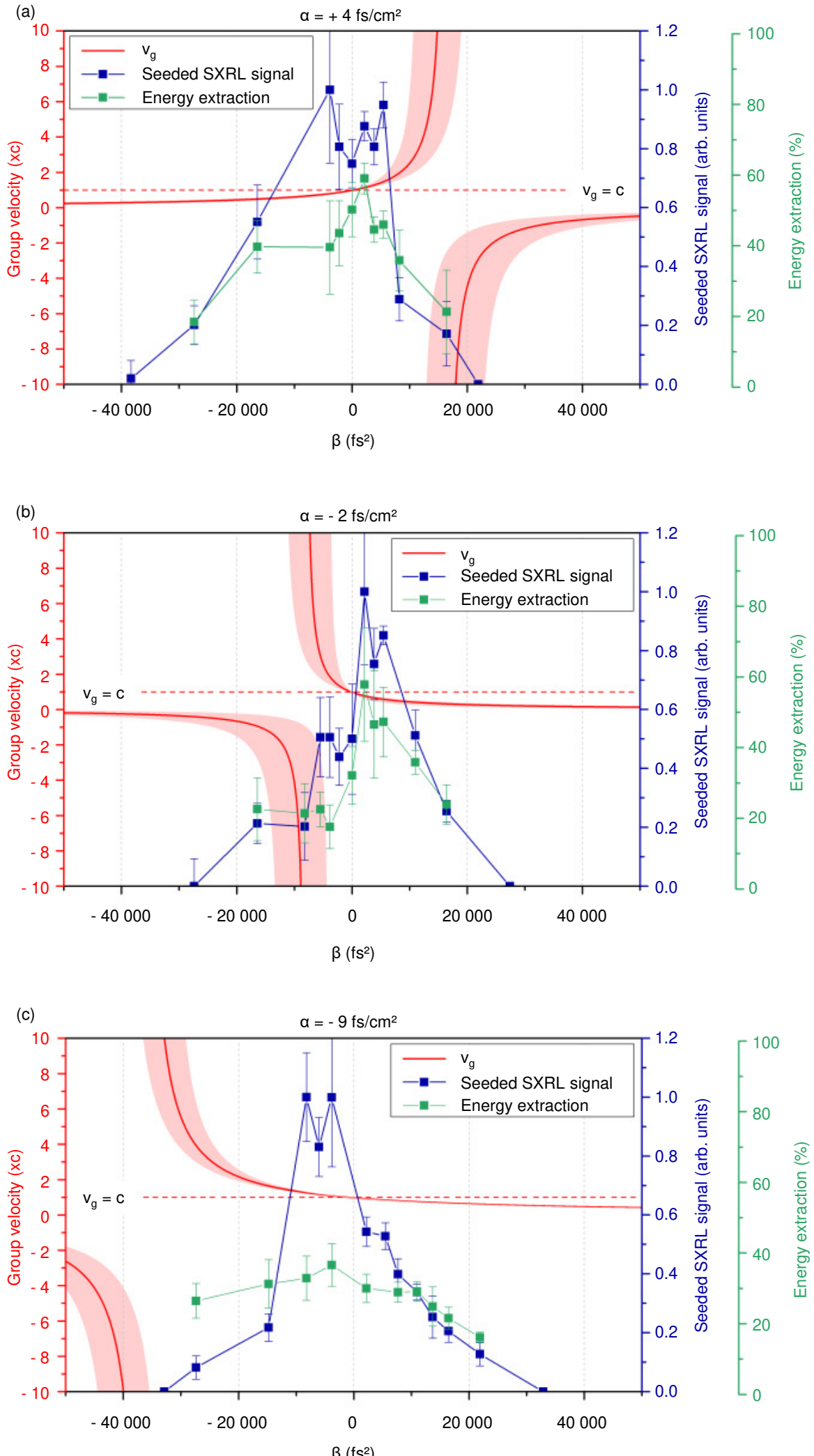
(a)
α = + 4 fs/cm²
v_g
Seeded SXRL signal
Energy extraction
v_g = c
Group velocity (xc)
Seeded SXRL signal (arb. units)
Energy extraction (%)
β (fs²)
(b)
α = - 2 fs/cm²
v_g
Seeded SXRL signal
Energy extraction
v_g = c
Group velocity (xc)
Seeded SXRL signal (arb. units)
Energy extraction (%)
β (fs²)
(c)
α = - 9 fs/cm²
v_g
Seeded SXRL signal
Energy extraction
v_g = c
Group velocity (xc)
Seeded SXRL signal (arb. units)
Energy extraction (%)
β (fs²)

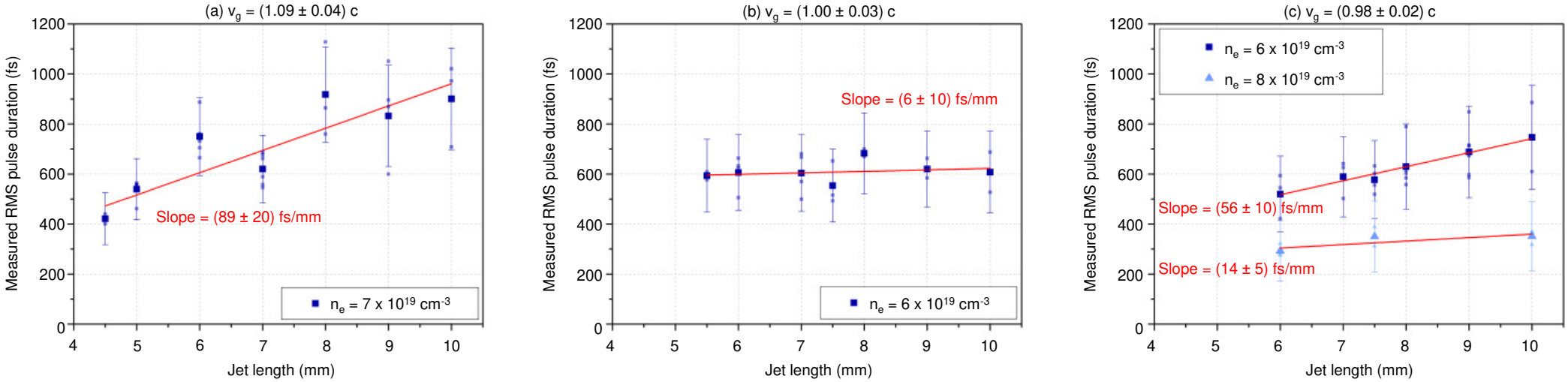
(a) v_g = (1.09 ± 0.04) c
Measured RMS pulse duration (fs)
Jet length (mm)
Slope = (89 ± 20) fs/mm
n_e = 7 x 10^{19} cm^{-3}
(b) v_g = (1.00 ± 0.03) c
Measured RMS pulse duration (fs)
Jet length (mm)
Slope = (6 ± 10) fs/mm
n_e = 6 x 10^{19} cm^{-3}
(c) v_g = (0.98 ± 0.02) c
Measured RMS pulse duration (fs)
Jet length (mm)
n_e = 6 x 10^{19} cm^{-3}
n_e = 8 x 10^{19} cm^{-3}
Slope = (56 ± 10) fs/mm
Slope = (14 ± 5) fs/mm

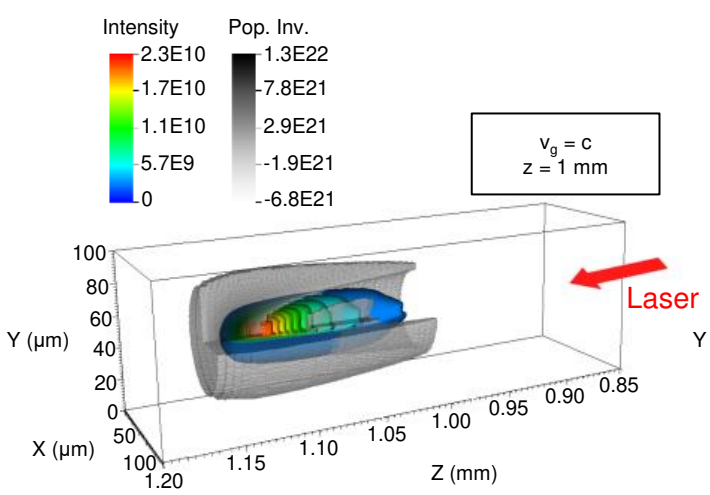
Intensity
2.3E10
1.7E10
1.1E10
5.7E9
0
Pop. Inv.
1.3E22
7.8E21
2.9E21
-1.9E21
-6.8E21
v_g = c
z = 1 mm
Laser
Y (μm)
X (μm)
Z (mm)

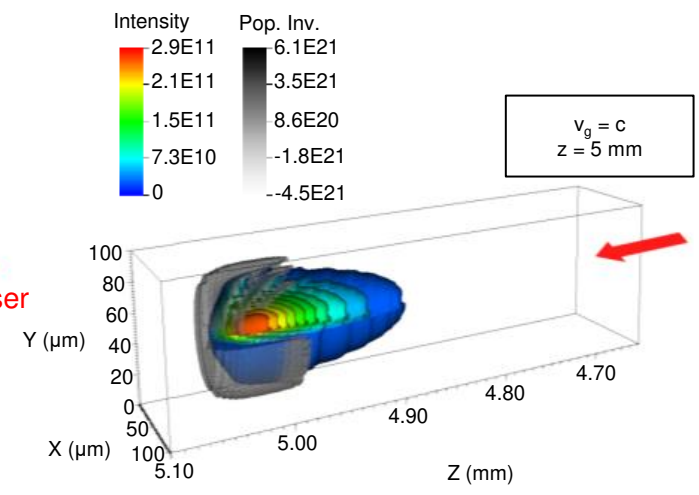
Intensity
2.9E11
2.1E11
1.5E11
7.3E10
0
Pop. Inv.
6.1E21
3.5E21
8.6E20
-1.8E21
-4.5E21
v_g = c
z = 5 mm
Y (μm)
X (μm)
Z (mm)

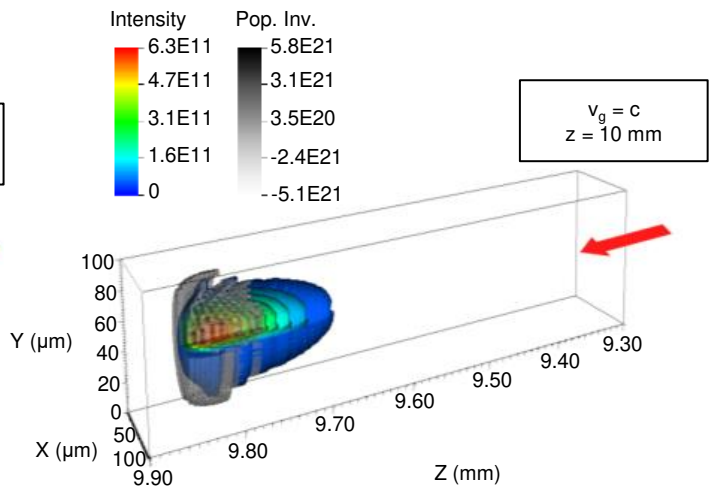
Intensity
6.3E11
4.7E11
3.1E11
1.6E11
0
Pop. Inv.
5.8E21
3.1E21
3.5E20
-2.4E21
-5.1E21
v_g = c
z = 10 mm
Y (μm)
X (μm)
Z (mm)

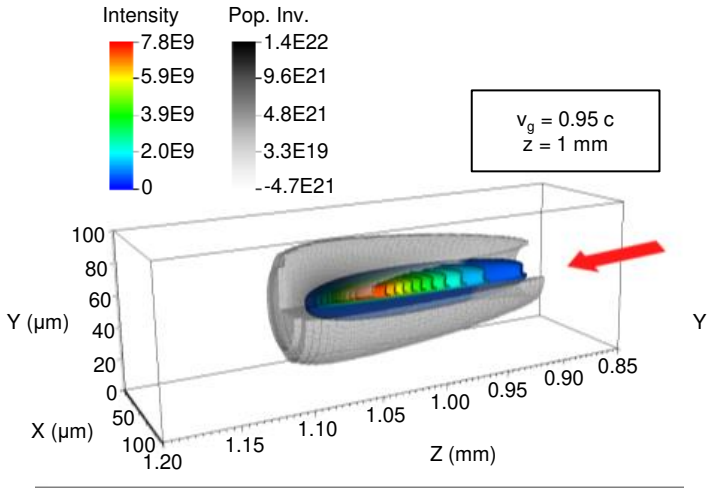
Intensity
7.8E9
5.9E9
3.9E9
2.0E9
0
Pop. Inv.
1.4E22
9.6E21
4.8E21
3.3E19
-4.7E21
v_g = 0.95 c
z = 1 mm
Y (μm)
X (μm)
Z (mm)

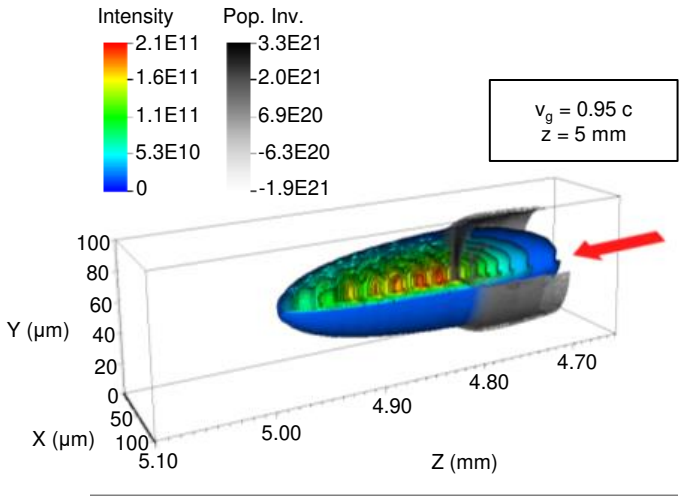
Intensity
2.1E11
1.6E11
1.1E11
5.3E10
0
Pop. Inv.
3.3E21
2.0E21
6.9E20
-6.3E20
-1.9E21
v_g = 0.95 c
z = 5 mm
Y (μm)
X (μm)
Z (mm)

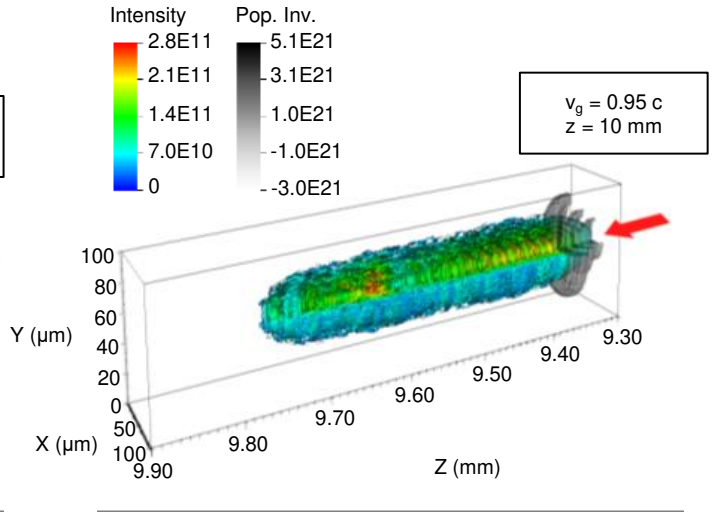
Intensity
2.8E11
2.1E11
1.4E11
7.0E10
0
Pop. Inv.
5.1E21
3.1E21
1.0E21
-1.0E21
-3.0E21
v_g = 0.95 c
z = 10 mm
Y (μm)
X (μm)
Z (mm)

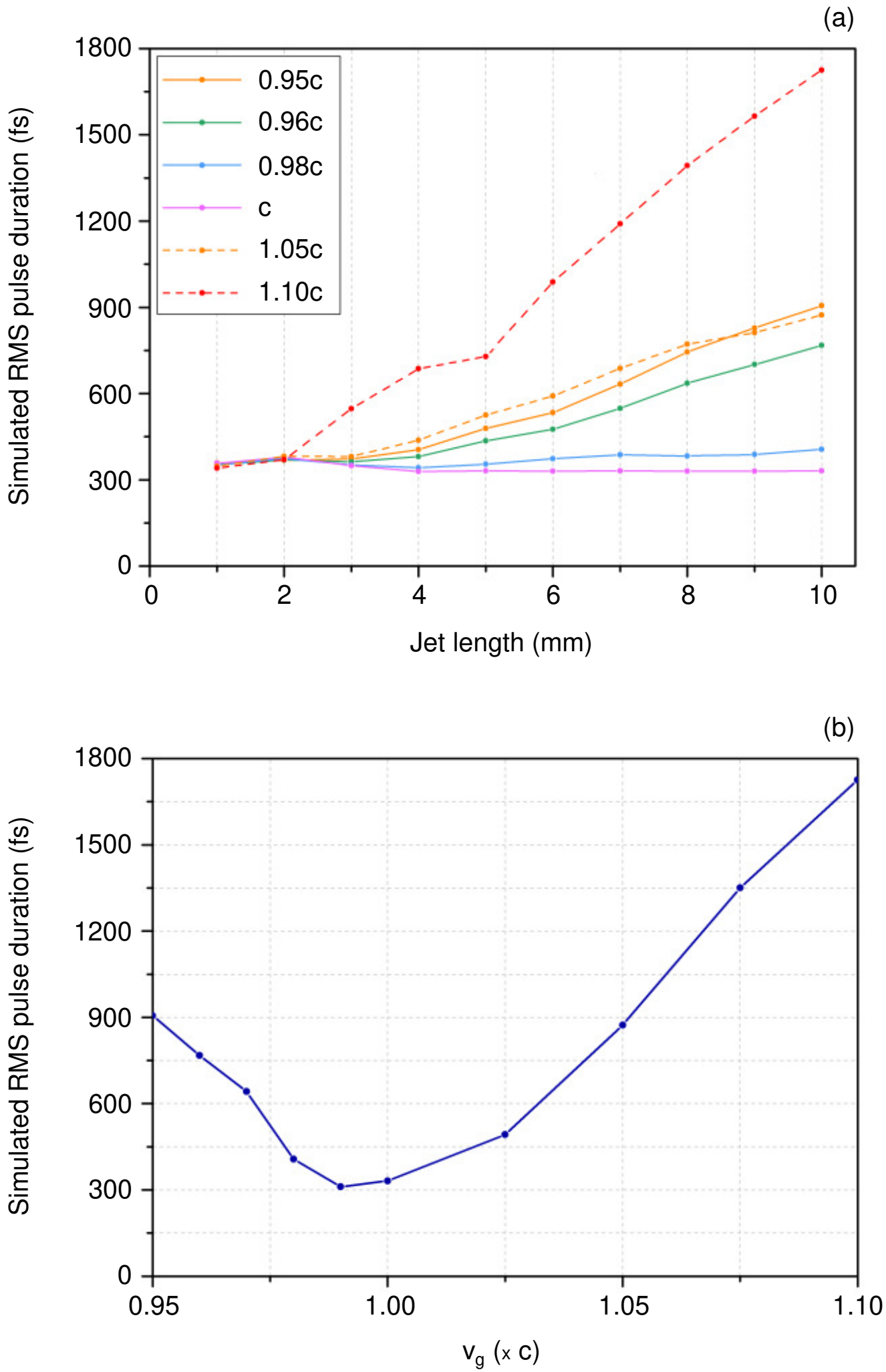
(a)
Simulated RMS pulse duration (fs)
1800
1500
1200
900
600
300
0
0.95c
0.96c
0.98c
c
1.05c
1.10c
0
2
4
6
8
10
Jet length (mm)
(b)
Simulated RMS pulse duration (fs)
1800
1500
1200
900
600
300
0
0.95
1.00
1.05
1.10
v_g (x c)